Journal of Systems Engineering and Electronics
Vol. 33, No. 3, June 2022, pp.563 – 574

Acquisition performance of B1I abounding with 5G signals

SHANG Peng[1,2,3], WANG Xue[4,*], ZOU Decai[1,5], CHU Ziyue[1,2,3], and GUO Yao[1,2,3]

1. National Time Service Center, Chinese Academy of Sciences, Xi'an 710600, China; 2. University of Chinese Academy of Sciences, Beijing 101408, China; 3. Key Laboratory of Precision Navigation and Timing Technology, Chinese Academy of Sciences, Xi'an 710600, China; 4. Institute of Information Sensing, Xidian University, Xi'an 710600, China; 5. School of Astronomy and Space Science, University of Chinese Academy of Sciences, Beijing 100049, China

Abstract: The widespread 5G base stations can be potential jammers for the vulnerable BeiDou B1I receivers due to its low power. Therefore, a novel analytical model is derived for the 5G signal to evaluate its impact on acquisition performance under three decision methods. The good agreement between the Monte Carlo method (MCM) through software defined receiver (SDR) and the derived expressions validates the effectiveness of the proposed algorithm. It can be found that the receivers exhibit varied responses for different 5G waveforms and decision strategies. The receiver also shows the least endurances for some kind of 5G waveforms, however, this kind of adverse effect can be cancelled by a reduced interference signal ratio (ISR), an increased integration time or a larger accumulation times.

Keywords: 5G new radio (NR), coexistence evaluation, acquisition performance, software defined receiver (SDR).

DOI: 10.23919/JSEE.2022.000024

1. Introduction

With the release of 3GPP R16, the industrial requirements for low latency and high reliability applications can be greatly satisfied, which will promote the prosperity of 5G infrastructures. There are plenty of 5G base stations all around the world and their number is expected to continue to grow in the following years. However, concerns are raised about its impact on the normal operation of the B1I receiver with a minimum reception power about 163 dBW[1].

Recent researches about 5G new radio (NR) compatibility can be summarized as two categories. Some researchers are interested in the influence of orthogonal frequency division multiplexing (OFDM) waveform on global navigation satellite system (GNSS) signals via practical tests. The long term evaluation (LTE) signal proposed by Light Square was rejected by the Federal Communications Commission (FCC) due to the severe performance degradation of various GPS receivers in real tests [2]. The influence of the third harmonics of DVB-T signals on GPS L1/Galileo E1 was also tested with the carrier to noise ratio (CNR) as an evaluation indicator [3]. The impact of LTE-machine to machine (LTE-M) second harmonics on GPS receivers was also evaluated in terms of its positioning error and CNR reduction. The results indicated that different receivers had varied tolerance to the interference power [4]. Another earlier research showed that the 4G signal in the S-band can lead to an obvious interference to BeiDou short messages, contributing to a significant CNR reduction [5]. A rough link budget between S-band 5G base stations and BeiDou terminals demonstrated that a proper isolation distance should be guaranteed for their green coexistence [6]. Practical measures between 5G NR transmitters and ultra wideband band (UWB) indicated the in-channel jammer can be detrimental to the maximum location range of UWB systems [7]. The results of coexistence for 5G and fixed services above 15 GHz manifested that the probability of interference can be minimized with the increased antenna directivity of the fixed links [8]. Similar findings were presented to analyze necessary protection requirements under 5G systems [9,10].

There are still some other developments focusing on some generic theoretical models to address the effect of different interferences on GNSS receivers. The effect of continuous wave, narrowband, broadband and pulse signals on GNSS acquisition and tracking were derived [11−14], however, it lacks practical application scenarios and its applicability to 5G waveform remains to be verified. The others concentrate on assessing the impact of interference through a software defined receiver (SDR) without giving too much insight about the nature of interference [15,16].

To the best knowledge of the authors, there has been little work on the compatibility assessment between 5G NR and the GNSS receiver in the L-band. Combing the

Manuscript received August 22, 2020.
*Corresponding author.

theoretical derivation with the SDR verification platform also motivates us to do this research, enabling a fast interference evaluation with flexible 5G waveform configuration.

Our research can benefit the coexistence evaluation between 5G NR and GNSS receivers, it can also be beneficial to combat the adverse impact of 5G NR for the receiver design.

The main contributions of this paper are as follows. Analytical expressions are derived to evaluate the effect of 5G NR broadband signals on B1I receivers with various waveform configurations in view of acquisition performance. The derived expressions are also evaluated through state-of-the-art acquisition decision strategies. Finally, measures are proposed to alleviate the potential interference between 5G NR and B1I signals in urban or rural areas with varied transmission distance.

The remainder of this paper is organized as follows. The signals under analysis are presented in Section 2. The derived expressions in terms of receiver operation characteristic (ROC) are depicted in Section 3. The comparison between simulation and theory is described in Section 4. Section 5 draws conclusions.

2. Signal and system model

The acquisition stage of the the B1I receiver is based on the correlation process between the received signal and the local replica, and its basic principles can be illustrated as Fig. 1.

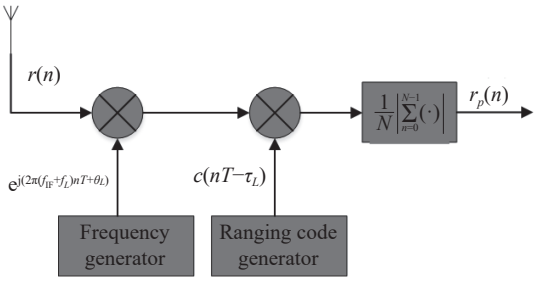

Fig. 1 Correlation process of the receiver

The received signal $r(n)$ includes three components, 5G NR signal, B1I signal and thermal noise, and the acquisition output amplitude $r_p(n)$ is obtained after the correlation process. $e^{j(2\pi(f_{IF}+f_L)nT+\theta_L)}$ is the replicated local carrier, and $c(nT-\tau_L)$ is the replicated ranging code. Their contributions to the correlator output will be derived in detail in the following subsections.

2.1 5G NR signal

Cyclic prefix (CP)-OFDM is chosen by the 3rd Generation Parter Project (3GPP) as the baseline waveform to support both downlink and uplink transmission. The closet adjacent band of 5G NR to B1I is n74 with a frequency range of 1 475 −1 518 MHz. According to the spectral mask definitions of TS 38.104 [17], the unwanted emissions into the B1I operating band belong to spurious emissions.

It seems that the 5G signal will have no impact on the B1I signal since there is enough frequency separation between them, however, it should be noticed that the transmitted power of 5G can be up to −6 dBW even for a local area base station, its power is much more higher than that of B1I. As demonstrated next, the 5G signal can impose potential threat on the B1I receiver in a certain frequency range and relative short transmission distance. Besides, similar findings in [2,18] indicated the potential interference in certain situations.

To address its effect on the receiver, the spurious emission limitation of the 5G signal and the path loss budget should be taken into account. All of these can be found in the relevant standards.

TS 38.104 specifies an equivalent spurious emission power limitation with −43 dBW, ITU-R M.2412 [19] stipulated comprehensive path loss models for different 5G application scenarios, and the enhanced mobile broadband (eMBB) is chosen here for its popularity.

The selected path loss models are urban macro (UMA) and rural macro (RMA) to describe the path loss of UMA cells as well as RMA cells respectively. The models are applicable to sub-6G band with a transmission distance no less than 10 m. The corresponding formulas were provided in [19].

When the distance is less than 10 m, the free space is adopted, the path loss coming free space with unmatched polarization can be achieved via

$$L = 32.45 + 20\lg f + 20\lg d + 3 \tag{1}$$

where L is in logarithmic units (dB), f is the operation frequency of 5G NR in linear units (MHz), d (km) is the separation between the base station and the B1I receiver.

Therefore, the piecewise path loss model of UMA and RMA can be obtained immediately. The theoretical path loss results for the above-mentioned models are depicted in Fig. 2 and Fig. 3. The related parameters are in line with ITU-R M.2142. The line of sight (LOS) and non-line of sight (NLOS) path loss in Fig. 2 and Fig. 3 are calculated by the theoretical model, and the expectation loss can also be computed by considering the probability of LOS.

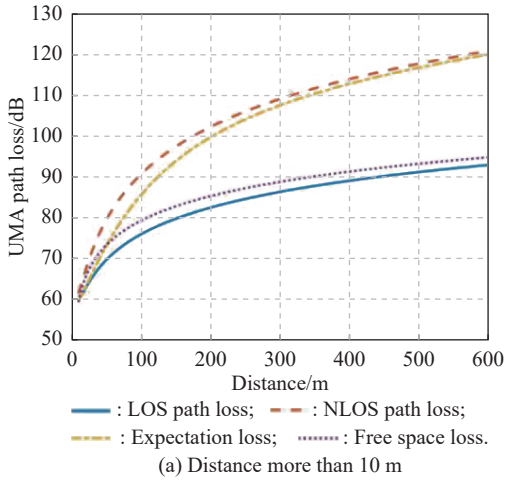

(a) Distance more than 10 m

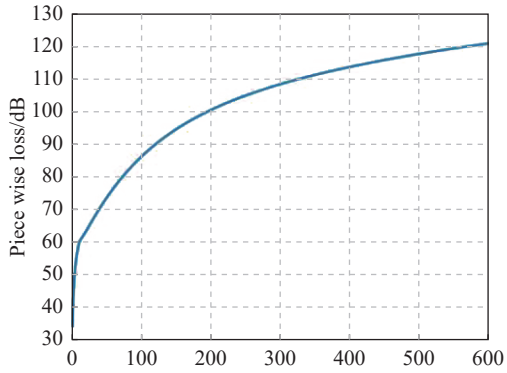

(b) Piece wise distance

Fig. 2 Pass loss of UMA model

Besides, comparing the expectation loss and the free space loss, it can be observed that the pass loss of the normally used free space model is much lower than the 5G path loss model when the distance is more than 100 m, leading to an overestimated interference evaluation to the B1I receiver. The piecewise path loss exhibits discontinuity at 10 m due to the applicable range of free space loss and expectation loss.

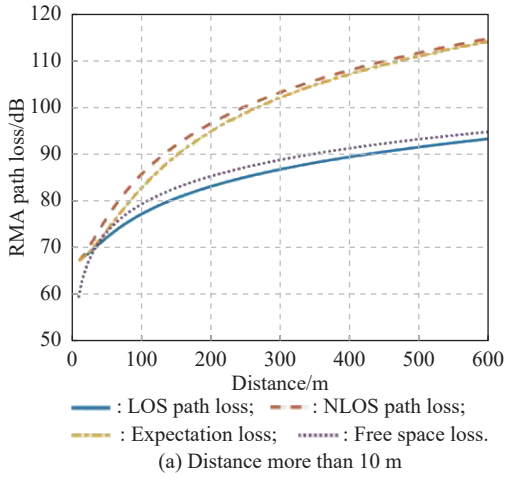

(a) Distance more than 10 m

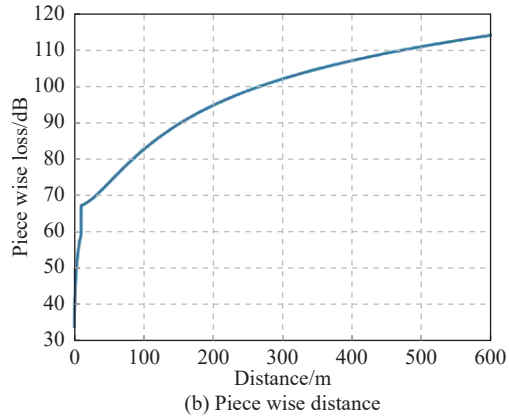

(b) Piece wise distance

Fig. 3 Pass loss of RMA model

The path loss results of the piecewise model for UMA and RMA at some specifics are given in Table 1 to facilitate our analysis.

Table 1 Piecewise path loss results

Path loss	Distance/m			
	5	10	125	165
UMA/dB	54	60	90	96
RMA/dB	54	56	86	91

It can be seen that the difference between UMA and RMA is within 6 dB, we choose UMA for the sake of brevity and the massively base stations in urban areas.

According to Table 1, when the distance is 125 m, the path loss is 90 dB, the incoming 5G NR spurious emission power will be −133 dBW, which is 30 dB higher than B1I. The considered distance in Table 1 is used to indicate the ratio between 5G spurious emission power and B1I, which is discussed in Section 4.

A simulated baseband 5G NR waveform compliant with the 3GPP specification is illustrated in Fig. 4. As it can be seen, its power spectral density (PSD) has a violent fluctuation, invalidating the flat PSD model.

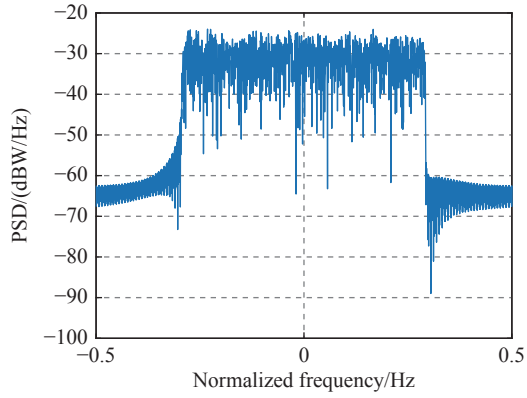

Fig. 4 PSD of CP-OFDM

Similar related findings [20] indicate a normally assumed flat spectrum could not well express the spurious

emission over a broad bandwidth.

Therefore, the PSD of CP-OFDM is adopted instead to better simulate the real situation.

For the sake of brevity, the PSD of CP-OFDM is given as follows, the detailed derivation can be found in [21]:

$$\Phi_{nr}(f)=P_{nr}T_{\text{tot}}\sum_{k=0}^{M-1}\left\{\text{sinc}\left[\left(f-\frac{k}{T_s}\right)\right]T_{\text{tot}}\right\}^2 \tag{2}$$

where P_{nr} is the power of a single OFDM subcarrier, T_s is the duration of an OFDM symbol, T_{tot} is the total symbol length, k is the index of the subcarrier, and M is the total number of subcarriers, sinc(x)=sin (πx)/(πx).

Therefore, the PSD of 5G signals is related to the modulation format, the subcarrier and the bandwidth. Based on the low pass feature of integration and dump operation, the power into the correlator can be obtained as

$$P_I=\int_0^{1/T_I}\Phi_{nr}(f)\,\text{d}f. \tag{3}$$

It may be hard to determine a closed form expression of (3), and this can be easily solved by a numerical integration.

After the above analysis, we can get the mathematical model for 5G NR waveform in the time domain as

$$I_{\text{NR}}(n)=\sqrt{P_I}\sum_{m=-BT_I/2}^{BT_I/2}\cos\left(2\pi\left(f_I+\frac{m}{T_I}\right)nT+\theta_I\right) \tag{4}$$

where T_I is the integration time, f_I is the interference frequency, B is the signal bandwidth, T is the sampling interval, and θ_I is the initial phase.

By filtering the spurious signal with a bandwidth of 4.092 MHz, the spurious emission of 5G signal is investigated. Therefore, it will influence all the spectral lines within the B1I signal main lobe. Its contribution to the correlator can be written as

$$s_{nr}=\sqrt{P_I}\frac{1}{N}\sum_{n=0}^{N-1}c(nT-\tau_L)\,\text{e}^{\text{j}(2\pi(f_{\text{IF}}+f_L)nT+\theta_L)}\cdot\sum_{m=-BT_I/2}^{BT_I/2}\cos\left(2\pi\left(f_I+\frac{m}{T_I}\right)nT+\theta_I\right) \tag{5}$$

where τ_L, θ_L, and f_L are the estimated code delay, the carrier phase, and the Doppler offset of the incoming signal respectively, f_{IF} is the intermediate frequency (IF) after conversion, and c is the ranging code.

The sum frequency terms in (5) are neglected due to the low pass trait of integration, leading to

$$s_{nr}=\sqrt{P_I}\frac{1}{N}\sum_{n=0}^{N-1}c(nT-\tau_L)\,\text{e}^{\text{j}(2\pi\Delta f_I nT)}\cdot\sum_{m=-BT_I/2}^{BT_I/2}\text{e}^{\text{j}(2\pi\,m/T_I nT+\Delta\theta_I)} \tag{6}$$

where Δf_I is the frequency error with $\Delta f_I=f_I-(f_{\text{IF}}+f_L)$, and $\Delta\theta_I$ is the phase error with $\Delta\theta_I=\theta_I-\theta_L$.

The ranging code in (6) can be expanded by Fourier series as

$$c(nT)=\sum_{k=-N_p}^{N_p}c_k\text{e}^{\text{j}2\pi\,k/T_p nT}. \tag{7}$$

The invariant normalized amplitude $c_k=1/2N_p$. Substitute (7) into (6), and the output amplitude of NR is given by

$$s_{nr}=\sqrt{P_I}\sum_{k=-N_p}^{N_p}\frac{1}{2N_p}\sum_{m=-BT_I/2}^{BT_I/2}\frac{1}{N}\sum_{n=0}^{N-1}\text{e}^{\text{j}2\pi\left(\left(\frac{k}{T_p}+\frac{m}{T_I}\right)nT\right)}\cdot\text{e}^{\text{j}\left(\Delta\theta_I+\varphi_k-k/T_p\tau_L\right)} \tag{8}$$

where T_P is the period of ranging code, N_p is its length, and φ_k is the phase.

The innermost summation can be obtained as follows by taking advantage of the property of geometric series:

$$\frac{1}{N}\sum_{n=0}^{N-1}\text{e}^{\text{j}2\pi\left(\left(\frac{k}{T_p}+\frac{m}{T_I}\right)nT\right)}=\text{sinc}\left(\left(\frac{k}{T_p}+\frac{m}{T_I}\right)T_I\right). \tag{9}$$

As T_I is a multiple of T_P, the summation can be written as

$$\sum_{m=-BT_I/2}^{BT_I/2}\text{sinc}\left(\left(\frac{k}{T_p}+\frac{m}{T_I}\right)T_I\right)=\begin{cases}1\,, & \dfrac{k}{T_P}+\dfrac{m}{T_I}=0\\ 0\,, & \text{otherwise}\end{cases}. \tag{10}$$

The summation can be calculated as follows by substituting the summation in (10) into (8):

$$\sum_{k=-N_p}^{N_p}\sum_{m=-BT_I/2}^{BT_I/2}\text{sinc}\left(\left(\frac{k}{T_p}+\frac{m}{T_I}\right)T_I\right)=2N_p. \tag{11}$$

Combining (11) with (8), the simplified expression is

$$s_{nr}=\sqrt{P_I}\sum_{k=-N_p}^{N_p}\text{e}^{\text{j}\left(\Delta\theta_I+\varphi_k-k/T_p\tau_L\right)}. \tag{12}$$

From the above derivation, it can be observed that the main factor affecting the output of the correlator is P_I, which is related to the modulation format, subcarrier, bandwidth, and integration time.

2.2 B1I signal

The B1I signal can be expressed as

$$s(t)=\sqrt{P_s}c(t-\tau_s)d(t-\tau_s)\cos\left((f_{\text{IF}}+f_D)nT+\theta_s\right) \tag{13}$$

where P_s is the nominal power of B1I signals, $c(t)$ is the ranging code, $d(t)$ is the navigation data, τ_s is the time delay, f_D is the Doppler offset, and θ_s is the carrier initial phase.

A zero padding technique[22,23] is adopted to counterbalance the frequent data transitions caused by the modu-

lated Neumann-Hoffman (NH) code on the navigation message.

Based on the contribution of B1I signals to the correlator, its output amplitude can be given by

$$s_s = \frac{1}{N}\sum_{n=0}^{N-1}\sqrt{P_s}c(nT-\tau_s)c(nT-\tau_L)\cdot \cos\left(2\pi((f_{\mathrm{IF}}+f_D)nT+\theta_s\right)\mathrm{e}^{\mathrm{j}(2\pi(f_{\mathrm{IF}}+f_L)nT+\theta_L)}. \quad (14)$$

Ignore the sum frequency term, and it can be furtherly simplified as

$$s_s = \sqrt{P_s}\frac{1}{N}\sum_{n=0}^{N-1}c(nT+\Delta\tau)\mathrm{e}^{\mathrm{j}(2\pi\Delta f_D nT+\Delta\theta)} \quad (15)$$

where $\Delta\tau=\tau_s-\tau_L$, $\Delta f_D=f_D-f_L$, and $\Delta\theta=\theta_s-\theta_L$.

The correlation in (15) can be approximated by an ideal auto-correlation function as follows when $\Delta\tau\leqslant T_a$:

$$\frac{1}{N}\sum_{0}^{N-1}c(nT+\Delta\tau)=\left(1-\frac{|\Delta\tau|}{T_a}\right). \quad (16)$$

Substituting (16) into (15) leads to

$$s_s = \sqrt{P_s}\left(1-\frac{|\Delta\tau|}{T_a}\right)\sum_{n=0}^{N-1}\mathrm{e}^{\mathrm{j}2\pi\Delta f_D nT}\mathrm{e}^{\mathrm{j}\Delta\theta}. \quad (17)$$

The summation in (17) can also be calculated with the same method as in (9), contributing to a concise expression as

$$s_s = \sqrt{P_s}\left(1-\frac{|\Delta\tau|}{T_a}\right)\mathrm{sinc}(\Delta f_D T_I)\mathrm{e}^{\mathrm{j}\Delta\theta}. \quad (18)$$

From (18), there is no doubt that there will be a distinct peak when the incoming signal and the replica are perfectly aligned.

2.3 Thermal noise

The thermal noise $w(nT)$ follows a zero mean normal distribution. A typical one side PSD value is represented by N_0, with the value of −204 dBW/Hz [24]. Therefore, the power of noise is −138 dBW, which is 25 dB higher than B1I.

Its contribution to the correlator can be written as

$$s_n = \frac{1}{N}\sum_{n=0}^{N-1}w(nT)c(nT-\tau_L)\mathrm{e}^{\mathrm{j}(2\pi(f_{\mathrm{IF}}+f_L)nT+\theta_L)}. \quad (19)$$

Therefore, s_n will follow a complex Gaussian distribution due to the multiplication with a complex exponential function. Its distribution can be written as follows due to the low pass filter with a bandwidth of $1/T_I$:

$$s_n \sim \mathrm{N}_c(0, N_0/(2T_I)). \quad (20)$$

3. Acquisition evaluation

The above derived expressions of (12), (18), and (20) can produce an aggregation effect on the correlator output, which can be expressed as

$$s = s_s + s_n + s_{nr}. \quad (21)$$

To evaluate the effectiveness of the derived expressions, an SDR-based evaluation framework in the perspective of receiver ROC is proposed in Fig. 5.

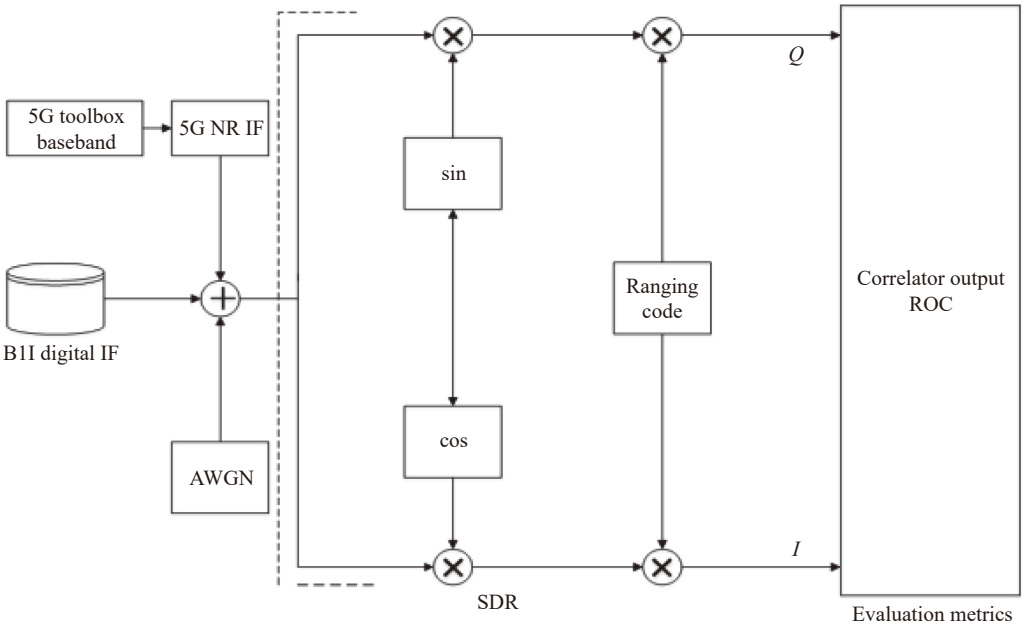

Fig. 5 Proposed framework of ROC

The 5G NR IF signal is to generate the 5G signal in compliance with the associated 3GPP standards by using the 5G toolbox [25], the digitized B1I IF signal is generated and additive white Gaussian noise (AWGN) is also added. The SDR part is the acquisition process by using the correlator to wipe off the carrier and the ranging code. The evaluation part is to quantify the effect of the 5G signal on ROC.

In general, the ROC curve is dependent on the adopted decision strategies to declare the presence or absence of the B1I signal. There are three state-of-the-art techniques to make such a decision. The decision is based on a binary hypothesis test, namely, the null hypothesis H_0 and the alternative hypothesis H_1, the binary hypothesis can be denoted as

$$\begin{cases} H_0 : s = s_{nr} + s_n \\ H_1 : s = s_s + s_{nr} + s_n \end{cases}. \tag{22}$$

The generalized likelihood ratio test (GLRT) [26,27] is to compare the maximum value of (21) to a given threshold β, so the detection probability and false alarm probability can be obtained as follows:

$$P_d = P(s \geqslant \beta | H_1) = \int_{\beta}^{+\infty} f_1(x|v,\sigma_n)\,\mathrm{d}x, \tag{23}$$

$$P_{\mathrm{fa}} = P(s > \beta, s_s = 0 | H_0) = \int_{\beta}^{+\infty} f_2(x|\sigma_n)\,\mathrm{d}x. \tag{24}$$

The mean and variance of the received signal are v and σ_n respectively. f_1 and f_2 are the corresponding probability density function (PDF) under hypotheses H_1 and H_0.

A similar GLRT method is employed with a modified predetermined threshold, and the threshold is the ratio of the maximum value to the mean value of (21) [28], which has a constant false alarm rate independent of the noise power.

Another widely used method is the maximum ratio test (MRT) proposed in [29], its main idea is to use the ratio of peaks as the test statistic and compare it with a prior threshold.

To determine the threshold, the distribution of H_0 or H_1 should be known as a prior knowledge, especially H_0 with a given false alarm probability. According to the Central Limit Theorem, the correlator output will follow a complex Gauss distribution with its mean and variance as outlined in (22).

The distribution of H_0 and H_1 in the presence of AWGN has been derived in the related literature, what we are interested in is that the contribution of 5G spurious signal to correlator output amplitude with the varied interference to signal ratio (ISR) and the 5G waveform. Take the GLRT decision for an example, the ROC can be formulated as follows:

$$\begin{cases} P_d = Q_1\left(\dfrac{v}{\sigma_n}, \dfrac{\beta}{\sigma_n}\right) \\ P_{\mathrm{fa}} = \mathrm{e}^{-\frac{\beta^2}{2\sigma_n^2}} \end{cases} \tag{25}$$

where Q_1 represents the marcum-q function. Similar derivations can be found in [28,29].

As can be seen in Fig. 8 and Fig. 9, there is an ISR turning point for different 5G waveforms, the main contribution of interference is to add the variance of (21) before that point. However, its main contribution is to increase the mean value after that.

Therefore, the derived analytical model of ROC can be obtained immediately by analyzing the contribution of the 5G spurious signal to the correlator statistic properties. The derived analytical expressions can also be verified by the Monte Carlo method (MCM) as the procedure shown in Fig. 5.

4. Simulation results and analysis

During the simulation, the effect of different 5G waveforms on B1I will be inspected, some measures are taken to eliminate the adverse effects on acquisition incurred by 5G signals.

The IF of B1I and 5G signals are set to 58.36 MHz and 15.36 MHz respectively, which is the frequency difference between the rightmost n74 frequency and the B1I signal, the sampling frequency is 245.76 MHz, the power of B1I is −163 dBW, the code delay and the Doppler offset of the B1I signal are assumed to be 1 023 chips and 200 Hz.

The 5G spurious signal is obtained by filtering the generated 5G signal with a nearly ideal filter whose center frequency and bandwidth is identical to B1I. Therefore, the ISR here is measured as the power ratio of the 5G spurious signal to B1I. The ISR considered here is 20−30 dB.

Besides, the 5G waveform can be characterized by its modulation format, sub-carrier spacing (SCS) and bandwidth, its general settings are listed in Table 2.

Table 2 Configuration of 5G waveforms

Parameter	Wave			
	1	2	3	4
SCS/KHz	15	15	30	30
Bandwidth/MHz	5	10	5	10
Modulation	16/64QAM			

The 5G NR waveform is an evolution of 4G waveform, which enables a variable and flexible SCS and diverse

modulation formats. The optional SCS for sub-6G eMBB can also be 60 kHz other than the SCS listed in Table 2, it is not chosen here for avoiding extra cyclic-prefix overhead. Quadrature amplitude modulation (QAM) is chosen for its prevalence as well as its superior outband spectral properties.

Firstly, a series of experiments are conducted to validate the effectiveness of the assumed complex Gaussian distribution as expressed in (21).

For the sake of brevity, the correlator output of the four waveforms listed in Table 2 are presented in Fig. 6 with only a 16QAM modulation and a 20 dB ISR, however, this also goes well for a 64QAM modulation and a higher ISR value we have considered.

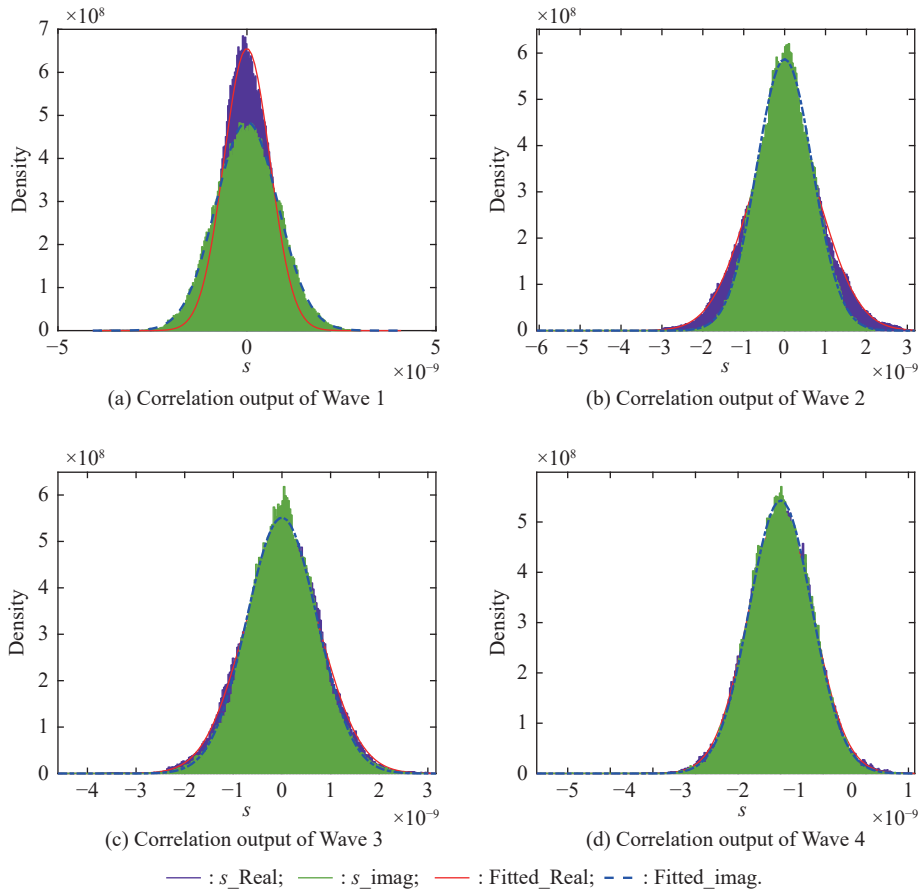

(a) Correlation output of Wave 1

(b) Correlation output of Wave 2

(c) Correlation output of Wave 3

(d) Correlation output of Wave 4

Fig. 6 Distribution of correlation output

As is illustrated in Fig. 6, the real and the imaginary parts of the correlation output can be well fitted by the normal distribution for all the four 5G waveforms, the returned values of performed goodness of fit tests are all zero at a significant level of 5%, confirming the assumed Gaussian distribution is accepted.

Secondly, some experiments are also performed to manifest the contribution of the 5G spurious signal to the correlation output.

The baseline of the correlator output amplitude in the absence of the 5G spurious signal and noise is presented as Fig. 7. The peak amplitude is in a good agreement with the theoretical value, namely, the square root of the power of B1I.

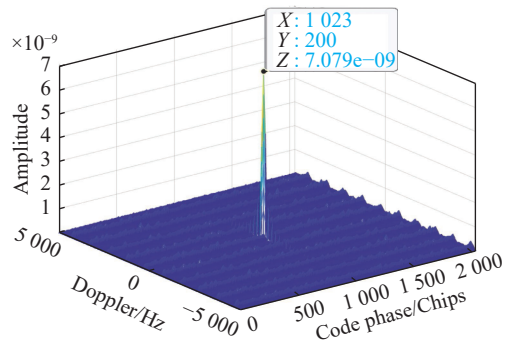

Fig. 7 Baseline acquisition output

A preliminary simulation is conducted to indicate the impact of varied ISR values of 5G waveforms on correlation, the correlation results of Wave 1 with ISR=20 dB and 30 dB are given in Fig. 8.

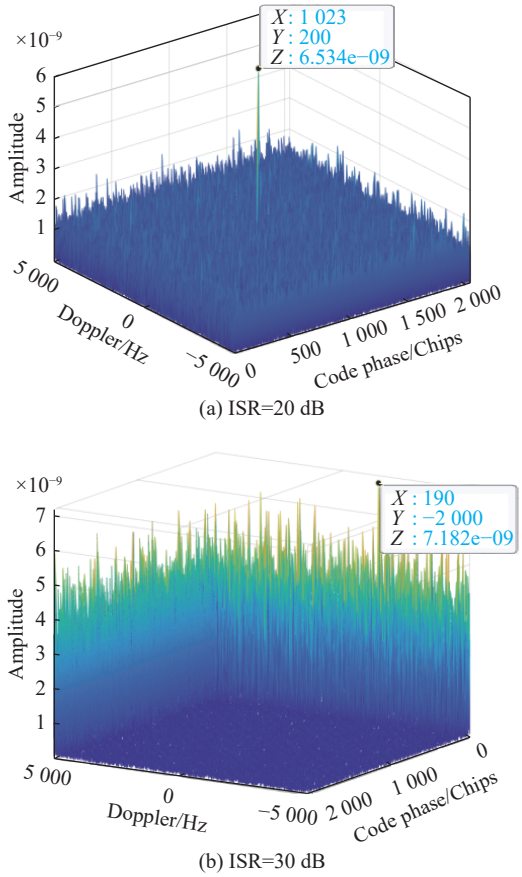

(a) ISR=20 dB

(b) ISR=30 dB

Fig. 8 Effect of ISR for Wave 1

As is shown in Fig. 8, when the ISR is 20 dB, a reduced peak can be observed which is caused by an increased variance of correlator output, however, the obvious interference peaks caused by an increased mean value of correlation can also be witnessed when the ISR is 30 dB. In fact, the effect of ISR on correlation output also holds for other 5G waveforms.

The detection probability of the three decision strategies under different 5G waveforms for the 16QAM modulation are given in Fig. 9, the false alarm probability is set to 0.01, the integration time is 1 ms and the non-coherent accumulation times is one.

The ISR effect of 5G waveforms among the decision methods indicates a great consistency. As is depicted in Fig. 9, the increasement of the ISR value will degrade the detection performance accordingly. Besides, the B1I receivers show the strongest and weakest endurance respectively when confronted with Wave 2 and Wave 3. The theoretical results are also in a good accordance with the simulation results. It can also be concluded that the GLRT decision outperforms MRT in all concerned 5G waveforms, while has a similar detection performance as the GLRT ratio decision method.

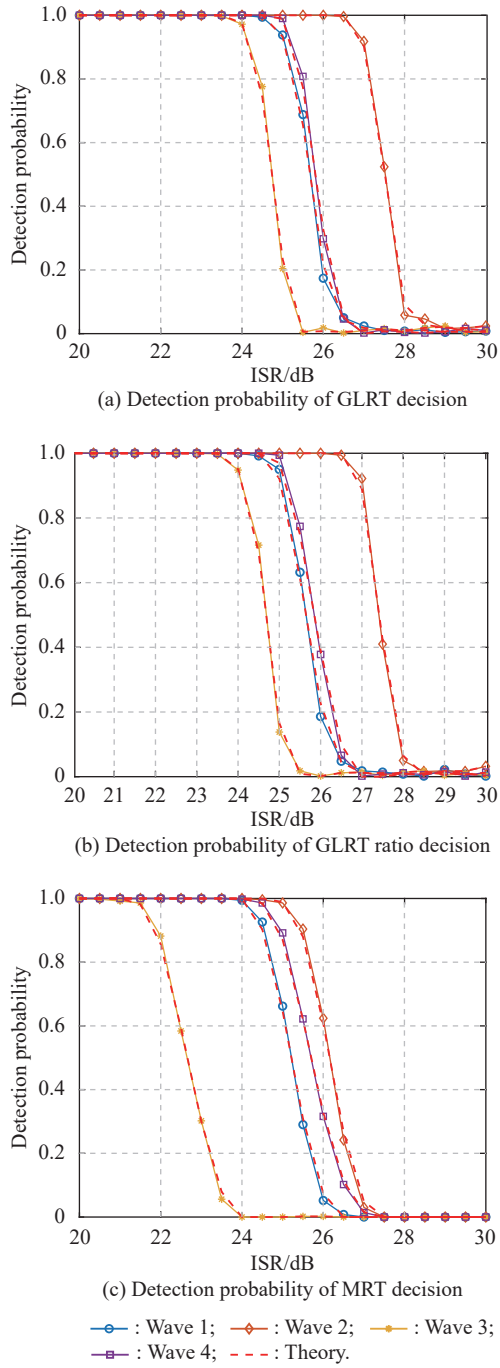

(a) Detection probability of GLRT decision

(b) Detection probability of GLRT ratio decision

(c) Detection probability of MRT decision

Fig. 9 Detection performance of decision methods for 16QAM modulation

In order to verify the correctness of the conclusions drawn from Fig. 9, the detection performance of 5G waveforms with 64QAM modulation is also presented in Fig. 10. The response of B1I receivers to 5G waveforms and the detection performance of the three decision strategies are the same as that in Fig. 9. The difference is that the B1I receivers demonstrate a varied tolerance for 5G waveforms with 64QAM compared with 16QAM.

Waveforms with 64QAM modulation has a higher detection probability other than Wave 1, which is caused by the spurious energy of the waveforms into the correlator.

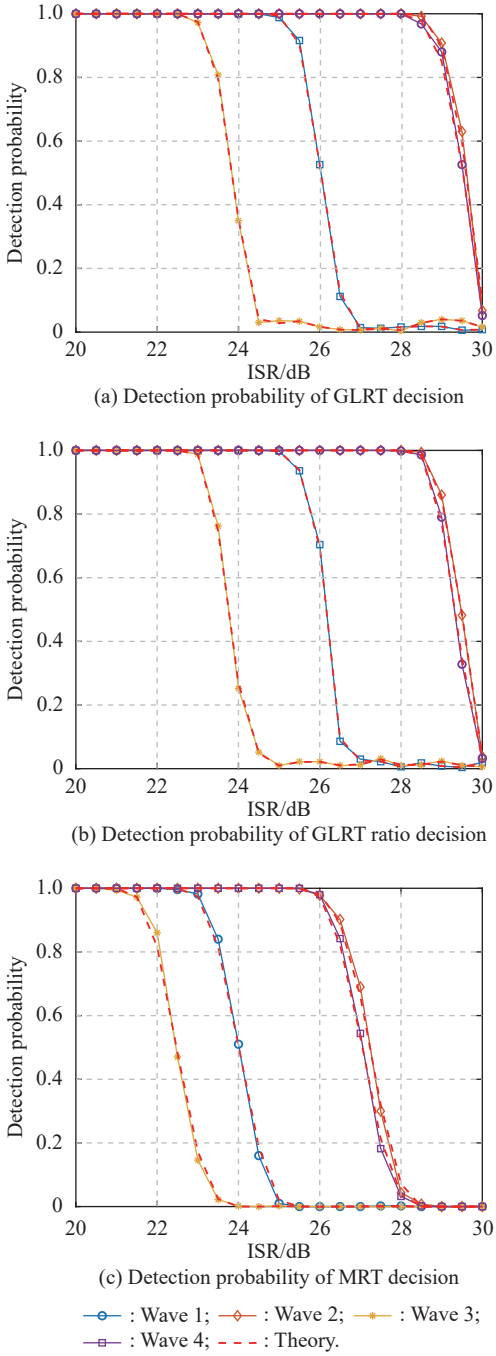

Fig. 10 Detection performance of decision methods for 64QAM modulation

It has been confirmed that the GLRT or the GLRT ratio decision strategy is superior to MRT regardless of the modulation scheme and waveform configurations of the 5G signal as shown in Fig. 9 and Fig. 10. Therefore, the ROC curve will be assessed under the GLRT and GLRT decision strategies.

The ROC curve is closely related to the ISR turning point, the ISR value is listed in Table 3.

Table 3 ISR turning point of 5G waveforms dB

Decision ISR waveform	Wave			
	1	2	3	4
GLRT	26	28	25	26
GLRT ratio	26	28	25	26

As has been stated above, the GLRT and GLRT ratio decision strategies have the similar detection performance, and the ISR point under these two decision methods are the same as in Table 3.

The ROC curve in terms of false alarm probability and detection probability is given in Fig. 11. The figure clearly shows that below the ISR turning point, the detection probability steadily increases as the false alarm probability increases, however, if the exerted ISR is above the turning point, the ROC curve will exhibit a distinct linear characteristic.

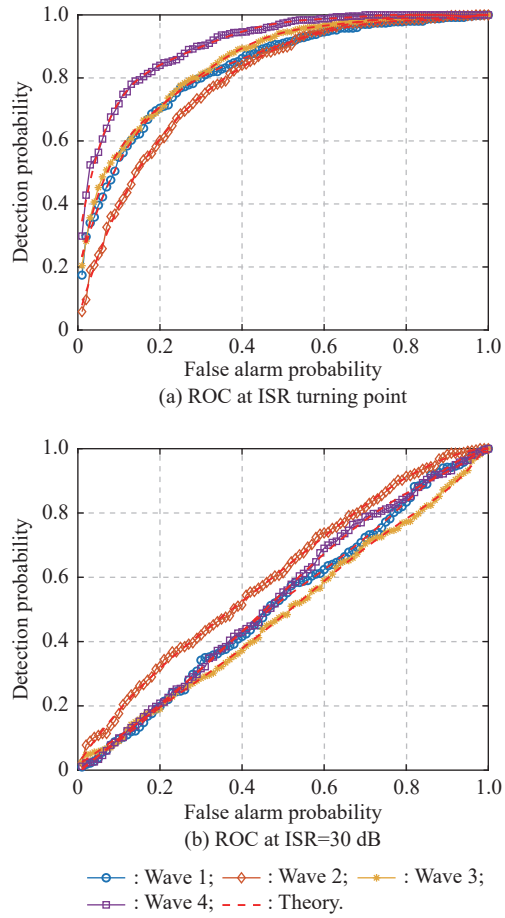

Fig. 11 Effect of ISR on ROC for GLRT

The results for the GLRT ratio are also described in Fig. 12, which furtherly validate the significant difference of the ROC curve around the ISR turning point. In reality, the steadily changing ROC curve results from the increase in the variance of correlation output, while the rapid linear change of the ROC curve stems from the increase of the mean value of the correlation output. This phenomenon can also be observed in [30].

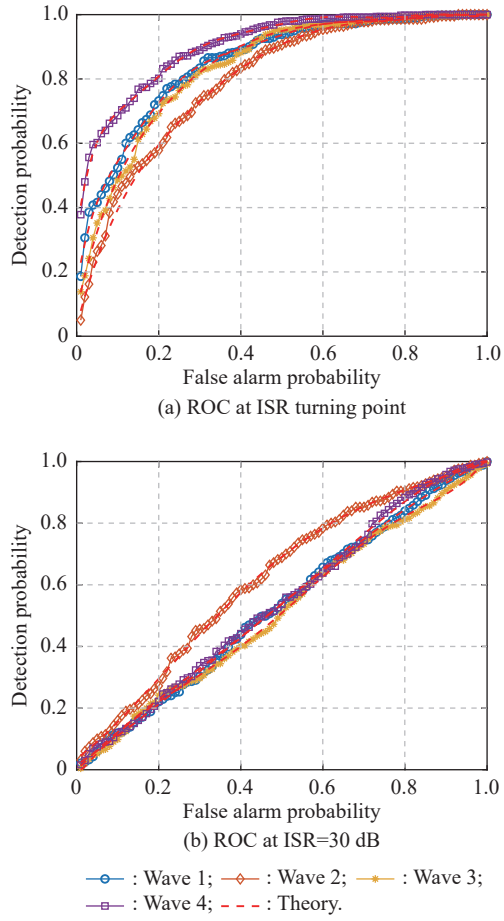

Fig. 12 Effect of ISR on ROC for GLRT ratio

All the above results verify the correctness of theoretical derivation by analyzing the contribution of 5G spurious signals to the statistical characteristics of the correlator output amplitude. It is also worth noting that there is unignorable detection performance degradation caused by 5G signals as shown in Fig. 9 and Fig. 10, therefore, some means can be taken to alleviate its adverse impact.

There are basically two insights to reduce its adverse effect. On one hand, the ISR value can be reduced by keeping a larger safety distance between 5G base stations and the GNSS receivers. As listed in Table 1, when the distance is 165 m, the imposed maximal ISR will be 24 dB, the detection performance in the presence of all considered waveforms are almost 100%. On the other hand, a longer integration time or a larger non-coherent accumulation times can improve the detection performance greatly, which are shown in Fig. 13 and Fig. 14.

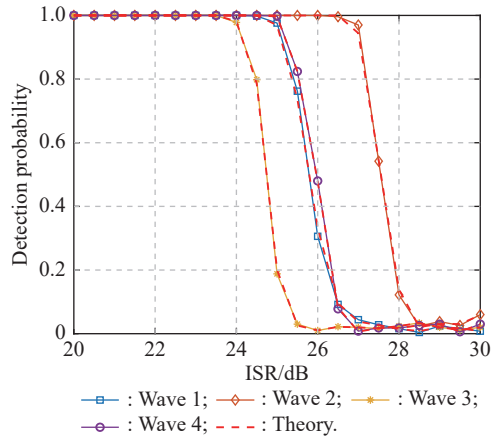

Fig. 13 Effect of integration time on detection

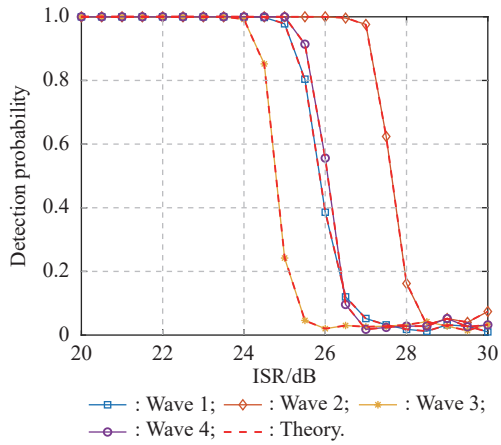

Fig. 14 Effect of non-coherent accumulation times on detection

The integration time in Fig. 13 is set to be 2 ms, compared with Fig. 9(a), the detection probability has increased from 94% to 98% for Wave 3 with ISR=24 dB, similar changes can also be observed for the other 5G waveforms. This is due to the fact that the variance of the noise floor and the spurious 5G signal can be greatly reduced by a longer integration time.

The simulation parameters in Fig. 14 are the same as Fig. 9(a) except the non-coherent accumulation times is 2, the detection probability has increased from 94% to 100% for Wave 3 with ISR=24 dB.

There is no doubt that a longer integration time or a larger accumulation times can improve the detection probability significantly as it is permitted.

In reality, some other measures can be adopted to relieve its effect in relative short transmission distance, the reason is that we chose the worst case situations with

the most adjacent 5G NR frequency in n74 band and the maximal spurious emission limitation.

In the above simulations, the equivalent radio frequency of the 5G signal is chosen as 1 518 MHz to simulate the worst case impact. To alleviate the potential effect caused by a transmission distance less than 10 m, it is suggested that the low end frequency of n74 should be utilized.

The effect of the frequency offset on ISR is displayed in Fig. 15. Take a frequency offset of 20 MHz as an example, it means that the equivalent radio frequency of 1 498 MHz is employed. It can be seen that when the frequency offset is 10 MHz, the minimum reduced ISR is 38 dB. According to Table 1, when the distance is 10 m, the imposed ISR will be 60 dB, therefore, the real ISR seen by the receiver will be 22 dB, which has little impact on the receivers. Similarly, when the frequency offset is 20 MHz, the minimum reduced ISR will be 47 dB, when the distance is 5 m, the real imposed ISR will be 20 dB, it will have no effect on the receivers in view of Fig. 9 and Fig. 10.

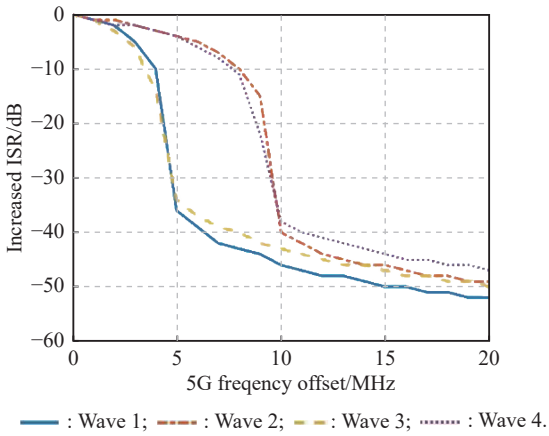

Fig. 15 Effect of frequency offset on ISR

Since the usable operating bandwidth is 20 MHz for n74 band, there must be an extremely short distance, which can not relieve its adverse effect by the frequency offset. However, its impact can still be reduced by a lower spurious emission power, which can be made by extra well-designed filters.

5. Conclusions

In this paper, we have derived the novel analytical expressions in terms of the effect of 5G spurious signals on the BeiDou B1I correlation process. The conducted simulations validate the correctness of the derivation. Some helpful insights can also be drawn to address their effect.

Firstly, the 5G waveforms with a narrower SCS and a wider bandwidth have the least impact on the receiver, whereas, the receiver suffers most with a wider SCS and narrower bandwidth 5G waveform. This phenomenon is independent of the modulation format or the adopted decision strategies.

Secondly, the detection performance of the acquisition with regard to the three decision strategies indicates that the GLRT-based decision approach is superior to the MRT method in all considered scenarios.

Thirdly, there is an ISR turning point determining the shape of the ROC curve for each 5G waveform. Especially, the ROC curve changes linearly with an ISR value above the turning point.

Finally, the 5G waveforms have little impact on the receivers when the distance is more than 165 m, when the distance is from 5 m to 165 m, the adverse effect can be cancelled by a longer integration time, an increased accumulation times or utilizing the low end frequency of n74 band. In some extremely short distance, i.e., less than 1m, additional filters can be employed to further lower its impact.

All in all, the n74 band of 5G signals imposes no threat to the B1I receiver in most situations, when the potential interference occurs, the above suggested measures can be taken to greatly relieve its impact. Our research can be extended to the modernized GNSS signals and the proposed analytical model can be furtherly improved.

References

[1] China Satellite Navigation Systems Management Office. BeiDou Navigation Satellite System Signal In Space Interface Control Document (V3.0). 2019. http://en.beidou.gov.cn/SYSTEMS/ICD/201902/P020190227702348791891.pdf

[2] O'DRISCOLL C, RAO M, BORIO D, et al. Compatibility analysis between LightSquared signals and L1/E1 GNSS reception. Proc. of the IEEE Position Location & Navigation Symposium, 2012: 447−454.

[3] WILDEMEERSCH M, RABBACHIN A, CANO E, et al. Interference assessment of DVB-T within the GPS L1 and Galileo E1 band. Proc. of the 5th ESA Workshop on Satellite Navigation Technologies and European Workshop on GNSS Signals and Signal Processing, 2010. DOI: 10.1109/NAVITEC.2010.5708046.

[4] APILO O, HIIVALA M, KUOSMONEN A, et al. Measured GPS performance under LTE-M in-device interference. Proc. of the 9th ESA Workshop on Satellite Navigation Technologies and European Workshop on GNSS Signals and Signal Processing, 2018. DOI: 10.1109/NAVITEC.2018.8642666.

[5] CHU H L, GAO Y, LU M Q. Test and analysis of the compatibility of S-band GNSS signal and its adjacent band signals. Journal of Telemetry, Tracking and Command, 2018, 39(3): 1–7.

[6] ZHANG H T. Analysis on spectrum interference coordination in 5G NR systems. Mobile Communications, 2019, 43(2): 38–42.

[7] CARFANO G, MURGUIA H, GUDEM P, et al. Impact of FR1 5G NR jammers on UWB indoor position location systems. Proc. of the International Conference on Indoor Positioning and Indoor Navigation, 2019. DOI: 10.1109/IPIN.2019.8911756.

[8] TERCERO M, SHARMA S, COLDREY M, et al. Coexistence

between 5G and fixed services. Proc. of the IEEE 83rd Vehicular Technology Conference, 2016. DOI: 10.1109/VTCSpring.2016.7504168.
[9] SON H K, CHONG Y J. Coexistence of 5G system with fixed satellite service Earth station in the 3.8 GHz band. Proc. of the International Conference on Information and Communication Technology Convergence, 2018: 1070−1073.
[10] KIM S, VISOTSKY E, MOORUT P, et al. Coexistence of 5G with the incumbents in the 28 and 70 GHz bands. IEEE Journal on Selected Areas in Communications, 2017, 35(6): 1254–1268.
[11] WANG P, WANG Y Q, YU X L, et al. Performance comparison of code discriminators in the presence of CW interference. Wireless Personal Communications, 2016, 89: 405–426.
[12] DAI X Z, NIE J W, LI B Y, et al. Performance of GNSS receivers with AGC in noise pulse interference. Proc. of the 5th International Conference on Computer Science and Network Technology, 2016: 735−740.
[13] BEK K M, SHANEEN M E, ELGAMEL S A. Mathematical analyses of pulse interference signal on post-correlation carrier-to-noise ratio for the global positioning system receivers. IET Radar, Sonar & Navigation, 2015, 9(3): 266–275.
[14] BEK K M, SHANEEN M E, ELGAMEL S A. Classification and mathematical expression of different interference signals on a GPS receiver. Navigation: Journal of The Institute of Navigation, 2015, 62(1): 23–37.
[15] ZHANG C, SHUI L, HUANG H, et al. Research on the mechanism and the impact of jamming on BeiDou software receiver. Proc. of the IEEE Chinese Guidance, Navigation and Control Conference, 2016: 198–202.
[16] JEONG S, SIN C S. GNSS interference signal generation scenario for GNSS interference verification platform. Proc. of the 15th International Conference on Control, Automation and Systems, 2015: 1363–1365.
[17] TS 38.104 V15.5.0. Technical specification group radio access network, base station (BS) radio transmission and reception. France: European Telecommunications Standards Institute, 2019.
[18] WEN R H, LIU Z J, SHEN J M. Compatibility analysis of the BDS and the 4G mobile communication system. Geomatics Science and Engineering, 2014, 34(4): 65–69.
[19] ITU-R Report M.2142-0. Guidelines for evaluation of radio interference technologies for IMT-2020. Geneva: Electronic Publication, 2017.
[20] STEPHEN M, HADI W, KAREN V D, et al. DOT GPS adjacent band compatibility assessment test results. Proc. of the International Technical Meeting of the Institute of Navigation, 2017: 637−661.
[21] PARK J, LEE E, PARK S, et al. Modeling and analysis on radio interference of OFDM waveforms for coexistence study. IEEE Access, 2019, 7: 35132–35147.
[22] LI Y F, SHIVARAMAIAH N C, AKOS D M. An open source BDS-3 B1C/B2a SDR receiver. Proc. of the ION ITM Institute of Navigation, 2018: 826–836.
[23] LI Y F, SHIVARAMAIAH N C, AKOS D M. Design and implementation of an open-source BDS-3 B1C/B2a SDR receiver. GPS Solutions, 2019, 23(60): 1–16.
[24] XIE G. Principles of GPS and receiver design. Beijing: Electronics and Industry Press, 2008.
[25] Mathworks. 5G Toolbox. https://www.mathworks.com/products/5g.html.
[26] GEIGER B C, VOGEL C, SOUDAN M. Comparison between ratio detection and threshold comparison for GNSS acquisition. IEEE Trans. on Aerospace and Electronic Systems, 2012, 48(2): 1772–1779.
[27] SLUMP C H, QUEK T Q S, RABBACHIN A. GNSS signal acquisition in harsh urban environments. Proc. of the IEEE International Conference on Communications Workshops, 2013: 62−67.
[28] ZIEMER R E, PETERSON R L. Digital communications and spread spectrum systems. New York: Macmillan and Collie, 2008.
[29] BORRE K, AKOS D M, BERTLSEN N, et al. A software-defined GPS and Galileo receiver: a single-frequency approach. New York: Springer, 2007.
[30] BENACHENHOU K, HAMADOUCHE M, TALEB-AHMED A. New formulation of GNSS acquisition with CFAR detection. International Journal of Satellite Communications and Networking, 2017, 35(3): 215–230.

Biographies

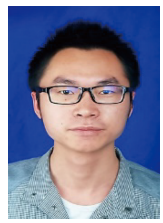

SHANG Peng was born in 1991. He received his M.S. degree in 2019 from the College of Electronic Information and Automation, Civil Aviation University of China, Tianjin. He is currently a Ph.D. candidate in the National Time Service Center. His research interests are compatibility assessment for intra and inter GNSS signals and intelligent signal processing for the identification of the communication transmitter.
E-mail: shangpeng19@mails.ucas.ac.cn

WANG Xue was born in 1979. He received his Ph.D. degree in telecommunication technology from the National Time Service Center, Chinese Academy of Sciences in 2011. Now he is a researcher at the Institute of Information Sensing, Xidian University. His research interests are GNSS signal quality monitoring and evaluation, GNSS signal design and verification, GNSS reception technology and anti-jamming, and detection and identification for the space signal.
E-mail: wangxue@ntsc.ac.cn

ZOU Decai was born in 1979. He received his M. S. and Ph.D. degrees in Telecommunication technology from the National Time Service Center, Chinese Academy of Sciences, in 2006 and 2009, respectively. He is a researcher of the National Time Service Center, Chinese Academy of Sciences. His current research interests include the development theory of satellite navigation, cooperative localization in wireless ad hoc networks, indoor positioning, and high precision time transfer navigation.
E-mail: zoudecai@ntsc.ac.cn

CHU Ziyue was born in 1996. He is currently an M.S. degree candidate at the National Time Service Center. His research interests are evaluation and feature extraction for the space signal.
E-mail: chuziyue@ntsc.ac.cn

GUO Yao was born in 1992. She is currently a Ph.D. candidate at the National Time Service Center. Her research interests are GNSS signal baseband algorithm and signal quality evaluation.
E-mail: guoyao@ntsc.ac.cn